Microfluidically Reconfigurable Mm-Wave Slow-Wave Phase Shifter with Integrated Actuation

Jonas Mendoza, *Student Member, IEEE,* and Gokhan Mumcu, *Senior Member, IEEE*

***Abstract*—A microfluidically reconfigurable slow-wave phase shifter (MRPS) with integrated actuation is introduced. MRPS is based on a selectively metallized plate (SMP) repositionable within a microfluidic channel placed in close proximity to a microstrip line. SMP repositioning creates a variable capacitive loading to alter the speed of the propagating wave. The device exhibits < 2 dB insertion loss (IL) and a reconfiguration time of 50 ms. The $|S_{21}|$, $|S_{11}|$, and phase performances are characterized to be stable with respect to gravity by no more than 0.16 dB, 3.02 dB, and 7.73° variations, respectively. Vibration test shows 0.08 dB in IL, 1.72 dB in return loss, and 4.23° in phase variations. The device is expected to handle 5.2 W of continuous RF power.**

***Index Terms*—Phase shifter, mm-wave, microfluidics, slow-wave, reconfigurable RF devices.**

I. Introduction

PHASE shifters (PSs) are key components of mm-wave phased antenna arrays [1]. Low-loss PSs are essential for efficiency, whereas PSs with high power handling capability can be critical for applications such as backhauling [2]. Mm-wave PSs in the literature are often based on CMOS [3], GaAs [4], and SiGe [5] technologies. However, their insertion losses (ILs) are high [6] with typical power handling on the order of 10 dBm. MEMS-based PSs have been reported with lower ILs (1-5 dB) [7]–[9] with power handling capability ~30 dBm.

More recently, microfluidics based device reconfiguration has attracted interest due to large frequency tuning and power handling. In these devices, liquid metals [10]–[12] and dielectrics [13] have been introduced to the vicinity of the device to reconfigure its RF response. A microfluidics based PS [14] has relied on circulating fluids with different dielectric constants and achieved a "phase shift"/ "IL" figure of merit (FoM) of ~9.36°/dB at 60 GHz. A recent PS [15] has also utilized the dielectric property of the circulating liquid to archive 9.28°/dB FoM at 0.9 GHz. On the other hand, utilization of liquid metals has remained much below the mm-wave band due to the challenges associated with actuation [16] and liquid metal oxidization [13] within channels that require lossy solutions for encapsulation [17]. In contrast to liquid metals, [18], [19] have utilized integrated actuation mechanism and selectively metallized plates (SMP) repositionable within microfluidic channels to demonstrate mm-wave switches and tunable filters. SMP has also been used in [20] to demonstrate a reflection type X-band PS; but, actuation was external and actuation distance/time was large (9.5 mm / 1.95 s).

Manuscript received May 12, 2022; accepted June 10, 2022. Date of current version July 21, 2022. This work was supported by the U.S. National Science Foundation under award 1920926. (Corresponding author: Gokhan Mumcu.)

The authors are with the Center for Wireless and Microwave Information Systems (WAMI), University of South Florida, Tampa, FL 33620 USA (e-mail: jonasmendoza@usf.edu; mumcu@usf.edu).

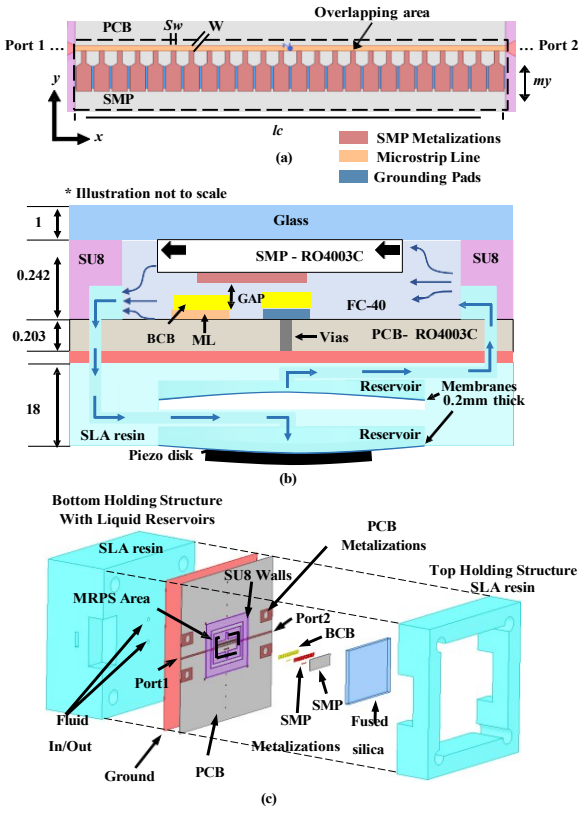

Fig. 1. MRPS structure and operation principle: (a) Exploded view; (b) Top view of SMP and PCB metallizations; (c) Substrate stack-up and vertically stacked liquid reservoirs loaded with piezoelectric disk.

This manuscript introduces a novel SMP based microfluidically reconfigurable phase shifter (MRPS) that operates at 28 GHz with integrated actuation and significantly reduced actuation time. As depicted in Fig. 1, SMP is encapsulated inside a photolithographically manufactured microfluidic channel made of SU8 (ϵ_r = 3.25 and tanδ = 0.0270) and sealed with fused silica to capacitively and periodically load a microstrip line patterned over a printed circuit board (PCB). The separation between SMP and PCB is kept constant by coating the PCB traces with a 6 µm thick Benzocyclobutene (BCB, Cyclotene 3022-46, ϵ_r = 2.65 and tanδ = 0.002). SMP and PCB metallization overlap areas are reconfigured by repositioning the SMP using liquid FC40 (ϵ_r = 1.9, tanδ = 0.0005), which has also been used in numerous prior work due to its low viscosity and dielectric loss [21] [22]. Compression and decompression of the fluid reservoirs under the device ground plane by a piezoelectric disk are used to actuate FC40 and reconfigure the SMP. The channel shape constraints SMP displacement to 100 μm, while different piezoelectric disk

actuation voltages can be used to generate a continuous phase difference. Section II covers the design of the MRPS. Section III presents the prototype and measured response. Specifically, MRSP exhibits <2 dB IL at 28 GHz with a >10 dB return loss (RL). It achieves reconfiguration within 50 ms. The device is characterized to handle 1 W of continuous RF power and is expected to handle up to 5.2 W. It operates with small deviations when subject to different orientations and vibration. A prototype is actuated 5 million cycles without damage.

II. MRPS Design

The substrate stack-up is from hard materials as shown in Fig. 1(b). 0.203 mm thick RO4003C substrates (ϵ_r = 3.55 and tanδ = 0.0027) are utilized for both the PCB and SMP. The sidewalls of the microfluidic channel are grown over the PCB using SU8 photoresist. Additionally, the top seal of the channel is a 1 mm thick fused silica substrate (ϵ_r = 3.28 and tanδ = 0.0005). The microfluidic channel walls are 242 μm tall. The design is initially carried out using Keysight Advanced Design System (ADS) Momentum suite with a 2D material approximation and validated in 3D by using Ansys HFSS.

The first design step is the microstrip line width. Similar to [23], the line impedance is taken high since capacitive loading will reduce its impedance. ADS's controlled impedance line tool is employed to determine the width of the line (w) as 0.12 mm for 78 Ω impedance. This implies a worst-case reflection of ≈ -10 dB when the line is terminated with 50 Ω. The line exhibits L' and C' (unit length inductance and capacitance) of 486.72 nH/m and 79.21 pF/m, respectively. A conductive pad that is 0.5 mm wide (0.2mm larger than the diameter of the vias) and a length as long as the device is placed near the microstrip line and grounded using vias. The distance between the pad and the line is reduced (0.35 mm) in a way to avoid changes in $|S_{11}|$ of the stand-alone line at 28 GHz. PCB also includes metallizations for edge connectors and interconnect lines for measurement (50 Ω with w = 0.42 mm).

The next design step is concerned with the unit cell (UC). As shown in Fig. 2, the UC consists of a microstrip line section (on PCB), a grounding pad section (on PCB), and a metallization trace (on SMP). The UC length is selected as 0.3813 mm, which is $1/15^{th}$ of a guided wavelength and suggests a per unit cell line capacitance and inductance of C = 0.0302 pF and L = 0.1856 nH. The section of the SMP trace that overlaps with the microstrip line (as SMP is repositioned along the y-axis with a displacement of my) creates capacitive loading per UC C_{added}. Similarly, the section of the SMP trace that overlaps with the grounding pad creates another capacitive loading per UC C_{grnd}. Using parallel plate capacitance approximation, the dimensions for the overlapping areas over the grounded traces of the PCB and the separation between PCB and SMP of 6 μm, C_{grnd} becomes 0.6257 pF. Additionally, taking into consideration that the total displacement of the SMP is limited to 0.12 mm (i.e. line width), and the width of the overlapping area is limited by 0.3 mm (to avoid mutual coupling among UCs), the maximum value of C_{added} is 0.1408 pF. The series connection of the two capacitors is the total loading, and it is therefore

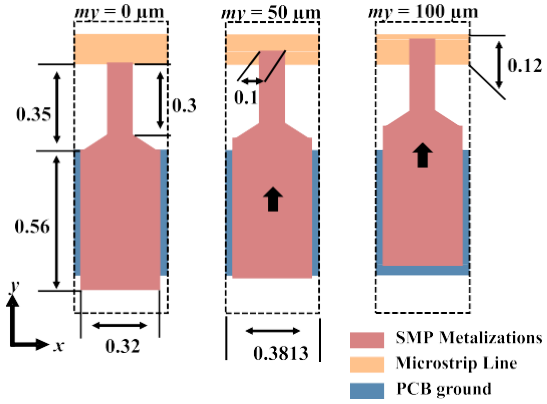

Fig. 2. Unit cell details for different SMP positions. From left to right: 0 µm, 50 µm and 100 µm. Dimensions are in mm.

approximately equal to C_{added}. The capacitance and inductance per UC of the MRPS becomes $C_{uc} \approx C_{added} + C'_{line_{uc}}$ and $L_{uc} = L'_{line_{uc}}$, respectively. Note that $C_{added} \neq 0$ for $my = 0$ due to the parasitic coupling. Fitting the LC circuit model to S-parameters of the UC simulated with ADS for $my = 0$ position shows that C_{uc} = 0.0363 pF which implies $C_{added_{min}}$ = 0.0061 pF. Equation (1) can be used to calculate maximum C_{uc} for the desired Bragg frequency. For this design, f_{Bragg} = 84 GHz (i.e. 3 × 28 GHz) that gives $C_{uc_{max}}$ as 0.0774 pF and $C_{added_{max}}$ as 0.0472 pF.

$$C_{uc_{max}} = \frac{1}{((f_{Bragg})^2(\pi)^2)(L_{uc})} \tag{1}$$

The following design step utilizes $C_{added_{max}}$ and $C_{added_{min}}$ in (2) to calculate the maximum overlapping area A as 0.01 mm^2. Assuming a square-shaped overlapping area for $C_{added_{max}}$ state, the width of the overlap area and the maximum my value become 0.1 mm as depicted in Fig. 2.

$$A = my^2_{max} = \frac{(C'_{added(Max)} - C'_{added(Min)})(d)}{(\epsilon_0\epsilon_r)} \tag{2}$$

The final design step is to determine the number of UCs required to attain 360° phase shift. By using comparison (such as a cascade of 15 and 14 unit cells), the phase shift per UC is estimated as 15.2° when my is changed from 0 to 0.1 mm. Therefore, the minimum number of UCs required to achieve 360° is 24, resulting in a total MRPS length l_c of 8.88 mm. The final dimensions are shown in Fig. 1 and Fig. 2.

III. MRPS Performance

The device is simulated with Ansys HFSS by including details pertaining to its 3D nature (SU8 walls, finite substrate size). Although the gap d between the SMP and PCB traces is deterministic in design as 6 µm, the fabrication tolerances place uncertainty. Therefore, parametric sweeps are also performed on d to correlate the simulated with the measured performance. The fabrication of the MRPS utilizes the process detailed in [24]. The functional footprint of the MRPS is 3 × 8.8 mm^2 while the total footprint including connectors and piezo actuation is 40 × 45 mm^2. The piezodisk utilized is a T216-A4NO-05 with a rated drive voltage of ±180 V.

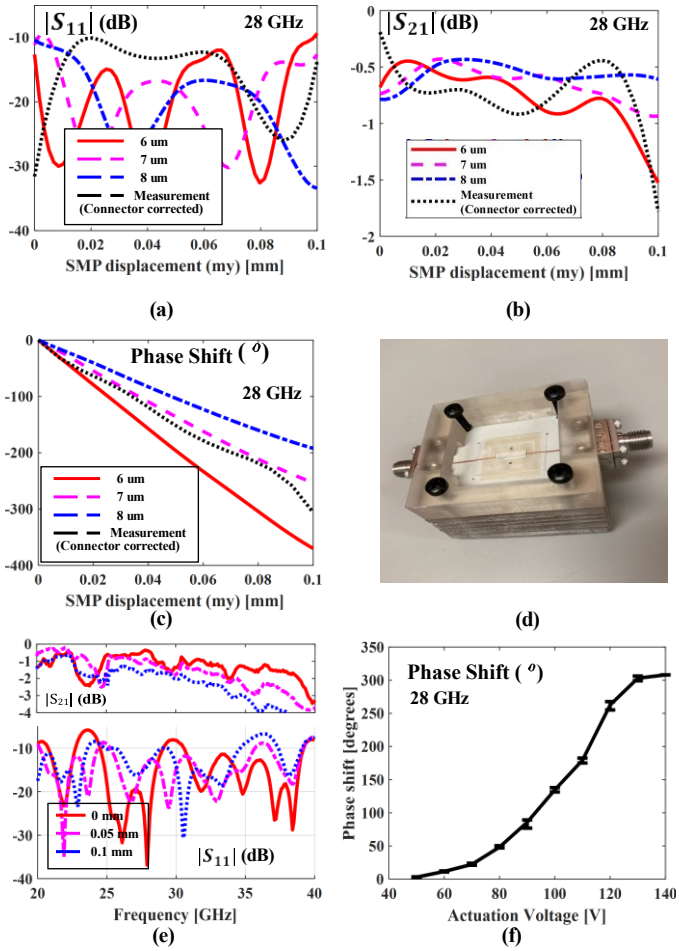

Fig. 3. (a) $|S_{21}|$, (b) $|S_{11}|$, and (c) Phase shift at 28 GHz; (d) Prototype; (e) Wideband response for my = 0 mm, 0.05 mm, and 0.1 mm; (f) Voltage vs Phase shift.

The actuation use vertically stacked reservoirs for achieving compact size. The reservoirs are placed at the backside of the PCB and constructed from ANYCUBIC 3D printing UV sensitive resin using a Stereolithography (SLA) printer. The larger size of the 3D printed holder allows for achieving stability during testing, which may be compromised due to cable weights on connectors. The device also exhibits an internal cavity represented as the absence of resin in Fig. 1(c) to allow unrestricted movement of the 3D printed inner membrane.

Fig. 3(a) shows the $|S_{11}|$ at 28 GHz. Simulated and measured $|S_{11}|$ are well matched to 50 Ω as *my* is varied from 0 to 0.1 mm. Fig. 3(b) presents $|S_{21}|$ at 28 GHz. The IL remains < 2 dB in simulated scenarios and measurements. Since simulations account for the MRPS operational area, the experimental results are compensated for connector and interconnect line losses. Fig. 3(c) depicts phase shift performance which is sensitive to *d*. The measured maximum phase shift is 305° and it is well predicted with d = 7 µm, which is very close to the design value of 6 µm. This fabrication accuracy issue can be resolved by adding ~ 5 unit cells in future prototypes. Fig. 3(d) shows the prototype used in experimental verification, while Fig. 3(e) shows the wideband measured response for *my* = 0 mm, 0.05 mm, and 0.1 mm. Additionally, the phase profile vs. actuation voltage with repeatability error bars is shown in Fig. 3(f) for 20 subsequent measurements. SMP position seems to be reset with a 0 V bias. However, a negative voltage is applied in tests to ensure *my* = 0 mm is achieved.

TABLE I
COMPARISON OF PS PERFORMANCES WITH THIS WORK*

Ref.	Tech.	Freq GHz	IL dB	PS °	FOM °/dB	P_{in} mW	Size mm^2
[3]	CMOS	11	8.3	360	32.72	6.5	1.195
[25]	MEMS	28	5.95	120	20.16	-	10.4
[26]	MEMS	25	2.34	360	153	-	-
[27]	SiGe	25	4.5	180	40	-	0.45
[28]	GaN	9	14	180	12.85	3000	23.5
[20]	µfl	9.5	0.95	360	379	5000	360
[15]	µfl	0.9	5.6	52	9.28	-	2040
*	µfl	28	1.8	305	170	5200	26.4

An initial prototype was also tested for reliability. The device remained functional after continuous operation of 6 days with actuation of 2×0.1 mm per cycle at a frequency of 10 Hz, for a total of 5 million cycles. The device speed was measured using an AmScope Microscope Digital Camera Model MU300, which has a limited resolution of 25ms between frames. The experimental setup shows total displacement in 2 frames, corresponding to a reconfiguration time less than 50 ms. This represents an improvement of 39× when compared against previous work in [20]. Actuation times in the order of ms could be attractive for applications requiring high power handling with low loss. Actuation time may be potentially decreased with SMP cross-section and design variations.

The effects of gravity on the device performance were studied with $|S_{21}|$, $|S_{11}|$, and phase measurements when the MRPS was facing up, down, and sideways. These resulted in 0.16 dB, 3.02 dB, and 7.73° deviations, respectively. Power handling capability is evaluated in simulations using ANSYS Workbench, predicting a maximum temperature of 155°C at the junction of the copper traces and the RO4003 PCB for 5.2 W of P_{in} at Port 1, which is the boiling point temperature for the FC40 liquid. Experimental verification of the thermal profile shows 26 C° while using 1W of constant RF power, which correlates well with simulations. Finally, Table I compares the MRPS presented in this document against recent state-of-the-art phase shifters. The presented PS has good performance with the lowest IL and highest power handling capability and best [PS]/[IL] at mm-wave bands.

IV. CONCLUDING REMARKS

A microfluidically reconfigurable phase shifter (MRPS) with integrated actuation is presented. The presented MRPS uses a 100 µm reconfiguration distance to provide 305° of phase range at 28 GHz band. Future work will consider alternative fabrication techniques to increase the speed of MRPS and support multiple simultaneous PS actuation for application in phased antenna arrays.

REFERENCES

[1] A. Valdes-Garcia, B. Floyd, S. T. Nicolson, J.-W. Lai, A. Natarajan, P.-Y. Chen, S. K. Reynolds, J.-H. C. Zhan, D. G. Kam, and D. Liu,

"A Fully Integrated 16-Element Phased-Array Transmitter in SiGe BiCMOS for 60-GHz Communications," *IEEE Journal of Solid-State Circuits*, vol. 45, no. 12, pp. 2757–2773, 2010. [Online]. Available: https://dx.doi.org/10.1109/jssc.2010.2074951

[2] Z. Gao, L. Dai, D. Mi, Z. Wang, M. A. Imran, and M. Z. Shakir, "MmWave massive-MIMO-based wireless backhaul for the 5G ultra-dense network," *IEEE Wireless Communications*, vol. 22, no. 5, pp. 13–21, 2015.

[3] S. Sim, L. Jeon, and J. Kim, "A Compact X-Band Bi-Directional Phased-Array T/R Chipset in 0.13 um CMOS Technology," *IEEE Transactions on Microwave Theory and Techniques*, vol. 61, no. 1, pp. 562–569 , ISSN = 1557–9670 , DOI = 10.1109/TMTT.2012.2 227 786, 2013.

[4] D. M. Zaiden, J. E. Grandfield, T. M. Weller, and G. Mumcu, "Compact and Wideband MMIC Phase Shifters Using Tunable Active Inductor-Loaded All-Pass Networks," *IEEE Transactions on Microwave Theory and Techniques*, vol. 66, no. 2, pp. 1047–1057 , ISSN = 1557–9670 , DOI = 10.1109/TMTT.2017.2 766 061, 2018.

[5] M. Sayginer and G. M. Rebeiz, "An Eight-Element 2–16-GHz Programmable Phased Array Receiver With One, Two, or Four Simultaneous Beams in SiGe BiCMOS," *IEEE Transactions on Microwave Theory and Techniques*, vol. 64, no. 12, pp. 4585–4597 , ISSN = 1557–9670 , DOI = 10.1109/TMTT.2016.2 620 144, 2016.

[6] C. W. Byeon and C. S. Park, "A Low-Loss Compact 60-GHz Phase Shifter in 65-nm CMOS," *IEEE Microwave and Wireless Components Letters*, vol. 27, no. 7, pp. 663–665, 2017.

[7] S. Dey and S. K. Koul, "Reliability Analysis of Ku-Band 5-bit Phase Shifters Using MEMS SP4T and SPDT Switches," *IEEE Transactions on Microwave Theory and Techniques*, vol. 63, no. 12, pp. 3997–4012 , ISSN = 1557–9670 , DOI = 10.1109/TMTT.2015.2 491 938, 2015.

[8] P. Edinger, C. Errando-Herranz, and K. B. Gylfason, "Low-Loss MEMS Phase Shifter for Large Scale Reconfigurable Silicon Photonics," pp. 919–921, 2019.

[9] W. Tian, Y. Zhang, M. Li, Z. Xie, and W. Li, "5-Bit Spiral Distributed RF MEMS Phase Shifter," pp. 94–98, 2019.

[10] B. D. Wiltshire, M. A. Rafi, and M. H. Zarifi, "Microwave resonator array with liquid metal selection for narrow band material sensing," *Scientific Reports*, vol. 11, no. 1, p. 8598, 2021. [Online]. Available: https://doi.org/10.1038/s41598-021-88145-3

[11] N. Vahabisani, S. Khan, and M. Daneshmand, "A K-Band Reflective Waveguide Switch Using Liquid Metal," *IEEE Antennas and Wireless Propagation Letters*, vol. 16, pp. 1788–1791, 2017.

[12] S. Khan, N. Vahabisani, and M. Daneshmand, "A Fully 3-D Printed Waveguide and Its Application as Microfluidically Controlled Waveguide Switch," *IEEE Transactions on Components, Packaging and Manufacturing Technology*, vol. 7, no. 1, pp. 70–80, 2017.

[13] V. Radonic´, S. Birgermajer, and G. Kitic´, "Microfluidic EBG Sensor Based on Phase-Shift Method Realized Using 3D Printing Technology," *Sensors (Basel)*, 2017.

[14] L. Le Cloirec, A. Benlarbi-Delai, and B. Bocquet, "3 bit 90^0 millimeter phase shifter using microfluidic technology," pp. 1161–1164, 2004.

[15] S. Choi, W. Su, M. M. Tentzeris, and S. Lim, "A Novel Fluid-Reconfigurable Advanced and Delayed Phase Line Using Inkjet-Printed Microfluidic Composite Right/Left-Handed Transmission Line," *IEEE Microwave and Wireless Components Letters*, vol. 25, no. 2, pp. 142–144, 2015.

[16] E. Gonza´lez and G. Mumcu, "Millimeter-Wave Beam-Steering Focal Plane Arrays With Microfluidically Switched Feed Networks," *IEEE Transactions on Antennas and Propagation*, vol. 66, no. 12, pp. 7424–7429 , ISSN = 1558–2221 , DOI = 10.1109/TAP.2018.2 874 488, 2018.

[17] K. Khoshmanesh, S.-Y. Tang, J. Y. Zhu, S. Schaefer, A. Mitchell, K. Kalantar-zadeh, and M. D. Dickey, "Liquid metal enabled microfluidics," *Lab on a Chip*, vol. 17, no. 6, pp. 974–993, 2017. [Online]. Available: http://dx.doi.org/10.1039/C7LC00046D

[18] E. Gonza´lez and G. Mumcu, "Integrated Actuation of Microfluidically Reconfigurable mm-Wave SPST Switches," *IEEE Microwave and Wireless Components Letters*, vol. 29, no. 8, pp. 541–544 , ISSN = 1558–1764 , DOI = 10.1109/LMWC.2019.2 925 889, 2019.

[19] E. Gonza´lez-Carvajal and G. Mumcu, "Frequency and Bandwidth Tunable mm-Wave Hairpin Bandpass Filters Using Microfluidic Reconfiguration With Integrated Actuation," *IEEE Transactions on Microwave Theory and Techniques*, vol. 68, no. 9, pp. 3756–3768, 2020.

[20] A. Qaroot and G. Mumcu, "Microfluidically Reconfigurable Reflection Phase Shifter," *IEEE Microwave and Wireless Components Letters*, vol. 28, no. 8, pp. 684–686 , ISSN = 1558–1764 , DOI = 10.1109/LMWC.2018.2 847 046, 2018.

[21] T. Palomo and G. Mumcu, "Microfluidically Reconfigurable Metallized Plate Loaded Frequency-Agile RF Bandpass Filters," *IEEE Transactions on Microwave Theory and Techniques*, vol. 64, no. 1, pp. 158–165, 2016.

[22] M. Azarmanesh, M. Dejam, P. Azizian, G. Yesiloz, A. A. Mohamad, and A. Sanati-Nezhad, "Passive microinjection within high-throughput microfluidics for controlled actuation of droplets and cells," *Scientific Reports*, vol. 9, no. 1, p. 6723, 2019. [Online]. Available: https://doi.org/10.1038/s41598-019-43056-2

[23] N. S. Barker and G. M. Rebeiz, "Optimization of distributed MEMS transmission-line phase shifters-U-band and W-band designs," *IEEE Transactions on Microwave Theory and Techniques*, vol. 48, no. 11, pp. 1957–1966 , ISSN = 1557–9670 , DOI = 10.1109/22.883 878, 2000.

[24] J. Mendoza, M. Karabacak, H. Arslan, and G. Mumcu, "A Spatially Adaptive Antenna Array for Mm-Wave Wireless Channel Control With Microfluidics Based Reconfiguration," *IEEE Access*, vol. 8, pp. 182 898–182 907 , ISSN = 2169–3536 , DOI = 10.1109/ACCESS.2020.3 028 795, 2020.

[25] T. Singh, N. K. Khaira, and R. R. Mansour, "Thermally Actuated SOI RF MEMS-Based Fully Integrated Passive Reflective-Type Analog Phase Shifter for mmWave Applications," *IEEE Transactions on Microwave Theory and Techniques*, vol. 69, no. 1, pp. 119–131, 2021.

[26] A. Borgioli, L. Yu, A. S. Nagra, and R. A. York, "Low-loss distributed MEMS phase shifter," *IEEE Microwave and Guided Wave Letters*, vol. 10, no. 1, pp. 7–9, 2000.

[27] C. C¸ alıs¸kan, M. Yazici, and Y. Gurbuz, "All-Pass Network and Transformer Based SiGe BiCMOS Phase Shifter for Multi-Band Arrays," *IEEE Transactions on Circuits and Systems II: Express Briefs*, vol. 68, no. 1, pp. 186–190, 2021.

[28] W. Luo, H. Liu, Z. Zhang, P. Sun, and X. Liu, "High-Power X -Band 5-b GaN Phase Shifter With Monolithic Integrated E/D HEMTs Control Logic," *IEEE Transactions on Electron Devices*, vol. 64, no. 9, pp. 3627–3633, 2017.